Supplemental Material for "Instability of metals with respect to strong electron-phonon interaction"

Emil A. Yuzbashyan,[1] Boris L. Altshuler,[2] and Aniket Patra[3]

[1]*Department of Physics and Astronomy, Center for Materials Theory, Rutgers University, Piscataway, NJ 08854, USA*
[2]*Physics Department, Columbia University, 538 West 120th Street, New York, NY 10027, USA*
[3]*Center for Theoretical Physics of Complex Systems, Institute for Basic Science, Daejeon 34126, Republic of Korea*

I. ELECTRONIC SPECIFIC HEAT

We define the grand canonical partition function for the electron subsystem as (in our units $k_B = \hbar = 1$)

$$\mathcal{Z}_{\rm el} = \frac{\mathcal{Z}}{\mathcal{Z}_{\rm ph}} = \frac{\mathrm{Tr}\, e^{-(\hat{H}-\mu\hat{N}_{\rm el})/T}}{\mathrm{Tr}_{\rm ph}\, e^{-\hat{H}_{\rm ph}/T}}, \tag{1}$$

where $\mathcal{Z}$ is the full partition function of the electron-phonon system and $\mathcal{Z}_{\rm ph}$ is the partition function of noninteracting phonons. This definition for the partition function of an interacting subsystem or, equivalently, of a system coupled to a bath (recall that phonons have a much larger heat capacity and effectively serve as a thermal bath for the electrons) arises naturally within the effective action approach [1–5]. As discussed in the introductory part of the main text, one should not renormalize the phonon frequencies within the ME theory but borrow them from ab initio calculations or experiment instead. For this reason, we take $\hat{H}_{\rm ph}$ in Eq. (1) to be the noninteracting phonon Hamiltonian but with the physical rather than bare phonon energies.

Accordingly, we define the electronic grand (Landau) potential $\mathtt{f}_{\rm el}$ per lattice site and the electronic specific heat $C_{\rm el}$ through

$$e^{-N\mathtt{f}_{\rm el}/T} = \mathcal{Z}_{\rm el}, \tag{2}$$

$$C_{\rm el} = -T\frac{\partial^2 \mathtt{f}_{\rm el}}{\partial T^2}, \tag{3}$$

where N is the number of lattice sites. It follows from these standard definitions that the total grand potential $\mathtt{f}$ and total specific heat C are

$$\mathtt{f} = \mathtt{f}_{\rm el} + \mathtt{f}_{\rm ph}, \quad C = C_{\rm el} + C_{\rm ph}, \tag{4}$$

where $\mathtt{f}_{\rm ph}$ and $C_{\rm ph}$ are the grand potential and specific heat of noninteracting phonons, respectively.

Since the specific heat of a metal C and the specific heat of noninteracting phonons $C_{\rm ph}$ are both well-defined and finite, $C_{\rm el} = C - C_{\rm ph}$ is free of any divergences when calculated correctly. Divergences discussed in [6–10] are merely artifacts of an inaccurate expression for $\mathtt{f}_{\rm el}$ on the Matsubara axis. We employed the zeta-function regularization procedure to obtain the correct answer [6–8] (see below), while [9] performed a cutoff regularization. In contrast, Prange and Kadanoff obtain the following answer on the real axis [11], which is divergence free from the beginning without any regularization (see also [12]):

$$\begin{aligned} C_{\rm el} &= 2\nu_0 \int dE\, E \left\{ \left[1 - \frac{\partial \Sigma}{\partial E}\right] \frac{\partial f_0}{\partial T} + \frac{\partial \Sigma}{\partial T}\frac{\partial f_0}{\partial E} \right\} \\ &= \frac{2}{3}\pi^2 \nu_0 T + \frac{2\nu_0}{T}\frac{\lambda\Omega}{2}\int dE d\tilde{E} \frac{\partial f_0(E)}{\partial E}\frac{\partial f_0(\tilde{E})}{\partial \tilde{E}} \\ &\quad \times \frac{(E-\tilde{E})^2}{E-\tilde{E}+\Omega}, \end{aligned} \tag{5}$$

where Σ is the equilibrium self-energy given by Eq. (4) of the main text with $f \to f_0$ and f_0 is the equilibrium Fermi distribution function. For simplicity, we specialized the second and third lines of Eq. (5) to Einstein phonons with energy Ω. To write down the answer for a general Eliashberg function, simply replace $\frac{\lambda\Omega}{2} \to \int_0^\infty d\omega \alpha^2 F(\omega)$ and $\Omega \to \omega$ in the denominator in the third line. Prange and Kadanoff derived Eq. (5) from the kinetic equation [Eq. (1) of the main text] by considering the change in the energy density ε of the electronic subsystem in response to a gradual change of temperature and using

$$\dot{\varepsilon} = \int dE E\{[1-\Sigma']\dot{f} + \dot{\Sigma} f'\}. \tag{6}$$

Note that there is a typo in [11] – the term in the square brackets in Eq. (5) should have the same sign as in the kinetic equation, i.e., minus rather than plus. Note also that with the help of Eqs. (5) and (6) and the chain rule, we immediately find the rate of change of the energy density for $f(E,t) = f_0(T(t))$ in terms of $C_{\rm el}$,

$$\dot{\varepsilon} = C_{\rm el}\dot{T}. \tag{7}$$

Prange and Kadanoff used this result to derive the expression (5) for $C_{\rm el}$ and we used it to obtain Eq. (16) of the main text.

Lee and Rainer showed [13] that Eq. (5) corresponds to the following expression for the Landau potential on the Matsubara axis:

$$\mathtt{f}_{\rm el} = -\frac{\pi^2\nu_0 T^2}{3} - \pi^2\nu_0 T^2 \lambda\Omega^2 \sum_{nm} \frac{\mathrm{sgn}(\omega_n\omega_m) - 1}{(\omega_n-\omega_m)^2 + \Omega^2}, \tag{8}$$

where $\omega_n = \pi T(2n+1)$ are the fermionic Matsubara frequencies, i.e., Eq. (5) obtains by differentiating Eq. (8) twice with respect to T, see Eq. (3). On the other hand, a straightforward evaluation of the continuous time path integral produces a divergent result [6–8]

$$\mathtt{f}_{\rm el} = -2\pi\nu_0 T \sum_n |\omega_n| - \pi^2\nu_0 T^2 \lambda\Omega^2 \sum_{nm} \frac{\mathrm{sgn}(\omega_n\omega_m)}{(\omega_n-\omega_m)^2+\Omega^2}. \tag{9}$$

Indeed, it is well known that the evaluation of path integrals without proper time slicing and a precise definition of the integration measure often results in badly divergent expressions [14–16]. This is already so for, e.g., free particles or a harmonic oscillator. The same divergences as in Eq. (9) arise in the Luttinger-Ward free-energy functional after integrating over the single-electron energy [13]. The way out is either to do the path integral correctly or to properly regularize the divergencies. Both approaches result in Eq. (8).

Clearly, not any regularization method will work. In particular, the cutoff regularization of Eq. (9) does not produce the right answer, in particular because the cutoff dependence does not cancel out. As Lee and Rainer point out [13]: "Obviously, the sum in (1) diverges, and cannot be regularized in a simple way, for instance by a frequency cut off." Here (1) refers to the low-temperature limit of our Eq. (9).

A well-known technique for dealing with divergent functional determinants is the zeta-function (a.k.a. analytic) regularization [14, 17–19], which does lead to the correct result [6–8]. Specifically, we manipulate the first term in Eq. (9) as

$$\begin{aligned} -2\pi\nu_0 T\sum_n |\omega_n| &= -4\pi^2T^2\nu_0\sum_{n=-\infty}^{\infty}\left|n+\frac{1}{2}\right| \\ &= -8\pi^2T^2\nu_0\sum_{n=0}^{\infty}\frac{1}{\left(n+\frac{1}{2}\right)^{-1}} \to -8\pi^2T^2\nu_0\zeta\left(-1,\frac{1}{2}\right) \\ &= -\frac{\pi^2\nu_0T^2}{3}, \end{aligned} \tag{10}$$

where $\zeta(s,a)=\sum_{n=0}^{\infty}\frac{1}{(n+a)^s}$ is the Hurwitz zeta function and we used $\zeta\left(-1,\frac{1}{2}\right)=\frac{1}{24}$. Another way to arrive at this result is to use the Poisson summation formula or convert the Matsubara sum to a contour integral with a suitable convergence factor [20].

In the second term in Eq. (9), we add and subtract 1 in the numerator. This results in a convergent expression [the second term on the RHS of Eq. (8)] plus a divergent extra term,

$$-\pi^2\nu_0T^2\lambda\Omega^2\sum_{nm}\frac{1}{(\omega_n-\omega_m)^2+\Omega^2}. \tag{11}$$

Applying the zeta-function regularization prescription to this term, we find

$$\begin{aligned} \pi^2T^2\sum_{nm}\frac{1}{(\omega_n-\omega_m)^2+\Omega^2} &= \frac{1}{4}\sum_{nm}\frac{1}{(n-m)^2+\left(\frac{\Omega}{2\pi T}\right)^2} \\ &= \frac{1}{4}\sum_L\sum_l\frac{1}{l^2+\left(\frac{\Omega}{2\pi T}\right)^2} = \sum_{L=-\infty}^{\infty}\text{const} \\ &= \text{const}\left[1+2\sum_{L=1}^{\infty}\frac{1}{L^0}\right] \to \text{const}[1+2\zeta(0)]=0. \end{aligned} \tag{12}$$

Here $L=n+m$, $l=n-m$ and we used $\zeta(0)=-\frac{1}{2}$. In fact, divergent Matsubara sums of the from $\sum_n \text{const}$ that regularize to zero are ubiquitous when evaluating functional integrals without proper time slicing, see, for example, p. 164 in [14]. We see that the zeta-function regularization does indeed produce the correct answer (8).

Lee and Rainer further evaluated Eq. (5) explicitly in terms of the digamma function $\psi(z)$ [13],

$$C_{\rm el}=\frac{2\pi^2\nu_0T}{3}\left[1-\lambda g\left(\frac{\Omega}{2\pi T}\right)\right], \tag{13}$$

where

$$g(x)=6x^2+12x^3\text{Im}[\psi^{(1)}(ix)]+6x^4\text{Re}[\psi^{(2)}(ix)], \tag{14}$$

where $\psi^{(1)}(z)$ and $\psi^{(2)}(z)$ are the first and second derivatives of the digamma function [$\psi^{(1)}(z)$ is also known as the trigamma function]. The digamma function enters through the equilibrium normal state self-energy. Indeed, evaluating $\Sigma[f]$ according to its definition [Eq. (4) of the main text] for $f=f_0(T)=[e^{\frac{E}{T}}+1]^{-1}$, we find

$$\Sigma=\frac{\lambda\Omega}{2}\text{Re}(\psi_+-\psi_-), \tag{15}$$

where $\psi_\pm=\psi\left(\frac{1}{2}+\frac{iE\pm i\Omega}{2\pi T}\right)$. Incidentally, we used this result to derive the equilibrium inverse quasiparticle weight function [Eq. (5) of the main text].

Let us estimate $\frac{|C_{\rm el}|}{C_{\rm ph}}$ at relevant temperatures for $\lambda\gtrsim 1$. We will employ the 3D Debye model for definiteness, even though a similar result holds in 2D and for Einstein phonons. We have $T_c>0.10-0.18\Omega$ for $\lambda\gtrsim 1$ [21–23], and we used $T=0.18\Omega$ as our lowest temperature in the main text. The phonon heat capacity at $T=0.18\Omega$ is $0.92N$, where N is the number of the ions [25]. According to Eq. (13), $C_{\rm el}\sim\frac{2\pi^2NT}{3E_F}$ assuming one conduction electron per ion. We conclude that indeed $|C_{\rm el}|/C_{\rm ph}\sim\Omega/E_F$ as stated in the main text, see also [7, 10].

Recently, Zhang *et al.* presented [10] one more calculation of $C_{\rm el}$ (for Einstein phonons in 2D) [24], which is overall similar to the one by Lee and Rainer [13]. Just as [13] it starts with the Luttinger-Ward functional and obtains the same well-known answer for $C_{\rm el}$ (see, e.g., [7, 26, 65]) that Lee and Rainer originally derived in [13], though the intermediate steps are not the same. In particular, an interesting feature of [10] is that the "counter term" (11) emerges naturally, while [13] merely suggests that it must arise from the phonon part of the Luttinger-Ward functional without providing further details.

In addition, Zhang *et al.* conjecture [10] that the normal state is stable even when $C_{\rm el}<0$ just because $|C_{\rm el}|$ is parametrically smaller than the phonon specific heat $C_{\rm ph}$ and the total specific heat $C_{\rm el}+C_{\rm ph}>0$. However, the smallness of $C_{\rm el}$ is not a valid argument in favor of stability. As a matter of fact, a system with a small negative heat capacity connected to another system (thermal bath) with positive and much larger in magnitude heat capacity (thus resulting in a positive total specific heat) is a textbook example of an absolute instability of this type [28–30]. The situation is more complicated in our case since the interaction between the electron and phonon systems is not weak. Due to this, a more detailed analysis of

the deviations from the the thermal equilibrium between the electrons and phonons, such as the one we performed in the main text, is necessary to prove or disprove the instability decisively.

In practice, the stability condition $C_{\rm el} > 0$ can be directly tested for any metal with a known Eliashberg function. The specific heat for a general $\alpha^2F(\omega)$ takes the form [13]

$$C_{\rm el} = \frac{2\pi^2\nu_0 T}{3}\left[1 - \int_0^\infty g\left(\frac{\omega}{2\pi T}\right)\frac{2\alpha^2F(\omega)}{\omega}d\omega\right], \quad (16)$$

with $g(x)$ given by Eq. (14). The requirement $C_{\rm el} > 0$ thus imposes a quantitative constraint on the Eliashberg function $\alpha^2F(\omega)$.

II. DETAILS OF THE LINEAR ANALYSIS

Recall that the linear kinetic stability analysis reduces to solving the generalized eigenvalue equation [Eq. (14) of the main text],

$$\gamma\int d\tilde{E}\, A_{\tilde{E}E}\varphi_{\tilde{E}} = \int d\tilde{E}\, M_{\tilde{E}E}\varphi_{\tilde{E}}. \quad (17)$$

The metal is stable when all generalized eigenvalues γ are positive and unstable when at least one of them is negative. The matrix (integration kernel) $A_{\tilde{E}E}$ reads

$$A_{\tilde{E}E} = -Z_0^{-1}f_0'\delta_{\tilde{E},E} + \sum_k \frac{\lambda_k\omega_k^2 f_0'\tilde{f}_0'}{(\tilde{E}-E)^2-\omega_k^2}, \quad (18)$$

and the matrix $M_{\tilde{E}E}$ in the case of the electron-phonon collision integral is $M = M^{\rm ep}$ and

$$M^{\rm ep} = \sum_k \lambda_k Q^k, \quad (19)$$

where (see also [31])

$$Q^k_{\tilde{E}E} = \frac{\omega_k}{T_0}N_0(N_0+1)\Big\{(f_0-\tilde{f}_0)\left[\delta_{\tilde{E},E-\omega_k} - \delta_{\tilde{E},E+\omega_k}\right] - \left[f_0(E+\omega_k) - f_0(E-\omega_k)\right]\delta_{\tilde{E},E}\Big\}, \quad (20)$$

$f_0 = f_0(E)$, $\tilde{f}_0 = f_0(\tilde{E})$, and $\delta_{X,Y} = \delta(X-Y)$. Whenever not shown, the temperature argument in equilibrium Bose (N_0) and Fermi (f_0) distributions functions is $T = T_0$. Observe that $Q^k_{\tilde{E}E}$ and therefore $M^{\rm ep}_{\tilde{E}E}$ are manifestly real symmetric. Keep also in mind that we rescaled the time variable $t \to \pi t$, which is equivalent to $\gamma \to \gamma/\pi$. Without this rescaling, an extra prefactor of π will appear in Eq. (20).

The matrix M is always positively defined, because the metal is obviously stable when the electron-phonon interaction is infinitesimally weak. Indeed, suppose $\lambda_k \neq 0$ only for one value of k, i.e., only the $k^{\rm th}$ phonon mode is present and λ_k is infinitesimally small. Since $M^{\rm ep} = \lambda_k Q^k$ is already proportional to λ_k, the contribution of the self-energy terms to the solution of the generalized eigenvalue equation are higher (second) order in λ_k. To determine the solution to the leading (first) order in λ_k, we need A only to the zeroth order. To zeroth order, $Z_0^{-1} = 1$ and $A_{\tilde{E}E} = -f_0'(E)\delta(\tilde{E}-E)$. This A is positively defined, since it is a diagonal matrix with a positive diagonal. Given that $\gamma > 0$ (the metal is obviously stable at weak coupling) and $\gamma A\cdot\varphi = \lambda_k Q^k\cdot\varphi$, it is an elementary exercise in linear algebra to show that Q^k is positively defined as well. But Q^k is independent of λ_k and since $M^{\rm ep}$ in Eq. (19) is a linear combination of positively defined matrices Q^k with positive coefficients, it is positively defined for *any* set of positive λ_k, i.e., for any physical Eliashberg function. For the same reason, the matrix $M^{\rm ee}$ obtained by linearizing the electron-electron collision integral must also be positively defined.

To determine the generalized eigenvalues γ numerically, we discretize the energy E in steps of ϵ and introduce a high energy cutoff $|E| \le \Lambda = L\epsilon$. We also fold the E-axis at $E = 0$ using $\varphi_{-E} = -\varphi_E$, since, as a consequence of the particle-hole symmetry, $f(-E) = 1 - f(E)$, and $\delta f(E)$ is therefore odd in E. This results in a matrix equation

$$\gamma A\cdot\varphi = M^{\rm ep}\cdot\varphi, \quad (21)$$

where A and M are $L\times L$ real-symmetric matrices. Explicitly,

$$A_{ij} = Z_0^{-1}(E_i)f_0'(E_i)\delta_{ij} - 4\epsilon\sum_k \lambda_k\omega_k^2 \times \frac{ij f_0'(E_i)f_0'(E_j)}{[(i-j)^2-r_k^2]\,[(i+j)^2-r_k^2]} \quad (22)$$

and

$$M^{\rm ep}_{ij} = \frac{N_0(N_0+1)}{T_0}\sum_k \lambda_k\omega_k\Big\{[f_0(E_{i-r_k}) - f_0(E_{i+r_k})]\delta_{ij} - [f_0(E_{i-r_k}) - f_0(E_i)]\delta_{j,i-r_k} - [f_0(E_i) - f_0(E_{i+r_k})]\delta_{j,i+r_k} + [1 - f_0(E_i) - f_0(E_j)]\delta_{j,r_k-i}\Big\}, \quad (23)$$

where $i,j = 1,\dots L$, $E_i = i\epsilon$, and $r_k = \frac{\omega_k}{\epsilon}$ are integers.

We determine γ by simultaneously diagonalizing matrices A and $M^{\rm ep}$. At weak coupling, the matrix A is positively defined and therefore all $\gamma > 0$. As we increase λ, the smallest eigenvalue of A vanishes at $\lambda = \lambda_c$. This implies that the largest in magnitude generalized eigenvalue $\gamma \to +\infty$ as $\lambda \to \lambda_c^-$ and $\gamma \to -\infty$ for $\lambda \to \lambda_c^+$. More specifically, $\gamma(\lambda)$ has a pole at $\lambda = \lambda_c$. In the main text, we formulated the criterion of instability as [Eq. (10) of the main text]

$$\min_E Z_0^{-1}(E) < 0, \quad (24)$$

i.e., λ_c is the value of λ for which the graph of $Z_0^{-1}(E)$ touches the E-axis. For λ close to λ_c, $\min_E Z_0^{-1}(E) \propto (\lambda_c - \lambda)$. Therefore, the largest in magnitude eigenvalue evaluated with the help of the approximate strong coupling expression [Eq. (11) of the main text] similarly shows a simple pole at $\lambda = \lambda_c$ as a function of λ.

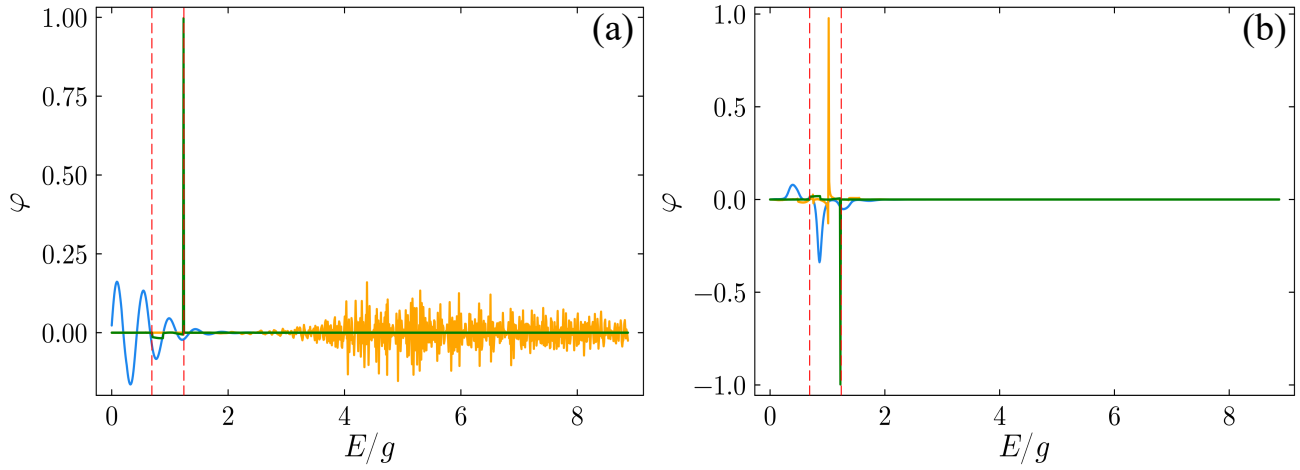

FIG. 1. Several representative eigenvectors $\varphi_E \equiv \varphi(E)$ of the linearized kinetic equation (17) in the unstable regime ($\lambda = 5.0 > \lambda_c = 1.48$). Panel (a) shows three stable eigenvectors and (b) three unstable ones. The corresponding eigenmodes exponentially decay (stable) or exponentially grow (unstable) with exponents γ. In both panels, the exponents γ_1, γ_2, and γ_3 corresponding to the eigenvectors shown in blue, orange, and green, respectively, satisfy $|\gamma_1| < |\gamma_2| < |\gamma_3|$. In fact, the green (blue) eigenvector in panel (a) corresponds to the largest (smallest) positive eigenvalue, whereas, in panel (b), the same color coding indicates the smallest (largest) negative eigenvalue. Note that unstable eigenvectors are localized in between the two zeros of $Z_0^{-1}(E)$ (shown with vertical dashed red lines), i.e., in the region where $Z_0^{-1}(E) < 0$. Phonon frequencies and couplings to the individual phonon modes are the same as for Table I.

While the criterion (24) holds with high accuracy, it is likely not exact due to the presence of the second term on the RHS of Eq. (18), which originates from the $f'\dot{\Sigma}$ term in the kinetic equation. However, this term is small due to the smallness of $f_0'(E)$ at the minimum of $Z_0^{-1}(E)$. As a result, it produces a relative error in λ_c of order 10^{-4} as compared to the instability criterion (24), see Table I. In fact, this error is so small that we cannot confidently discern whether the $Z_0^{-1}(E)$ criterion is exact or not within the accuracy of our numerics.

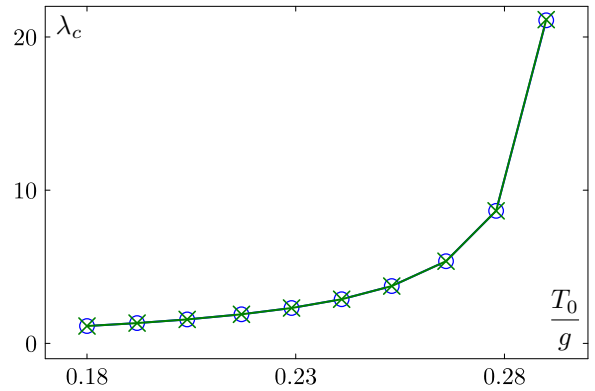

FIG. 2. Critical values λ_c of the electron-phonon coupling vs the equilibrium temperature T_0. For $\lambda > \lambda_c$, the metal is unstable with respect to small deviations from the thermal equilibrium between the electrons and phonons. Green crosses obtain from the instability criterion $\min_E Z_0^{-1}(E) < 0$ and blue circles from the linear stability analysis. Note that these two methods produce visibly indistinguishable results. $Z_0(E)$ is the quasiparticle weight function. Phonon frequencies are $\omega_k = (39+k)\epsilon$ with $\lambda_k = \frac{\lambda}{21}$, where $k = 1, 2, \ldots, 21$ and ϵ is the discrete energy step.

T_0	λ_c(Linear Analysis)	λ_c(Minimize Z_0^{-1})	$\delta\lambda_c/\lambda_c$
0.180	1.1335	1.1333	1.8×10^{-4}
0.192	1.3262	1.3253	6.8×10^{-4}
0.204	1.5644	1.5644	$< 10^{-4}$
0.217	1.8991	1.8980	5.8×10^{-4}
0.229	2.3096	2.3094	0.9×10^{-4}
0.241	2.8822	2.8820	0.7×10^{-4}
0.253	3.7427	3.7416	2.9×10^{-4}
0.266	5.3639	5.3642	-0.6×10^{-4}
0.278	8.6508	8.6517	-1.0×10^{-4}

TABLE I. Comparison of $\lambda_c(T_0)$ values obtained from the full linear stability analysis and from the instability condition $\min_E Z_0^{-1}(E) < 0$ [Eq. (24)]. Phonon frequencies ω_k and couplings to the individual phonon modes λ_k are the same as in Fig. 2.

Let us note that the matrix A is indefinite for $\lambda > \lambda_c$, and, as a result, some of its eigenvalues vanish in the continuum limit $\epsilon \to 0$. The corresponding γ therefore diverge. For discrete energies such divergent eigenvalues occur at a discrete set of values of the coupling λ [see Fig. 2 of the main text]. To see this, first neglect the small second term on the RHS of Eq. (18). Then, A is diagonal and its eigenvalues are $-Z_0^{-1}(E)f_0'(E)$. For $\lambda > \lambda_c$, $-Z_0^{-1}(E)$ always has two zeroes, which are generally in between of the grid points. The pole-like divergencies seen in Fig. 2 happen when one of the zeros snaps to the grid, i.e., coincides with one of the E_i.

In Fig. 1, we also show a few representative stable and unstable eigenvectors for $\lambda > \lambda_c$. All unstable eigenvectors are localized between the two zeros of $Z_0^{-1}(E)$ in the region where $Z_0^{-1}(E) < 0$. Furthermore, the eigenvectors corresponding to the largest positive (for $\lambda < \lambda_c$) and the smallest negative (for $\lambda > \lambda_c$) γ are always localized in the vicinity of

the same real root of $Z_0^{-1}(E)$. Note that these eigenvectors are responsible for the pole-like divergence at $\lambda = \lambda_c$.

We did not use the explicit form of the electron-electron collision integral and the corresponding matrix $M^{\rm ee}$ in this paper. The following two properties of the electron-electron collisions are important for our proof: (1) they conserve the total energy of the electronic subsystem and (2) $M^{\rm ee}$ is real symmetric. Property (1) reflects energy conservation – in the absence of interactions with the phonons (with the thermal bath) the total energy of the electrons is conserved. Property (2) manifests itself thanks to the substitution $\delta f = -f_0'\varphi$ [Eq. (12) of the main text], see also, e.g., the related discussion in [32]. In addition, we have verified both these properties for an explicit example – electron-electron collisions in weakly disordered conductors. The collision integral in this case reads [33]

$$I_{\rm ee}(E) = -\frac{1}{\pi}\int d\omega \int d\tilde{E} P(\omega) R^{\omega}_{E\tilde{E}}, \tag{25}$$

where

$$\begin{aligned} R^{\omega}_{E\tilde{E}} = {} & f_E f_{\tilde{E}-\omega}(1-f_{E-\omega})(1-f_{\tilde{E}}) \\ & - f_{E-\omega} f_{\tilde{E}}(1-f_E)(1-f_{\tilde{E}-\omega}), \end{aligned} \tag{26}$$

$f_E \equiv f(E,t)$ is the electron distribution function, and $P(\omega)$ is the transition probability. Importantly, $P(\omega)$ is even in ω. The extra factor of $\frac{1}{\pi}$ in Eq. (25) as compared to the expression in [33] is due to our rescaling $t \to \pi t$. Observe that $I_{\rm ee}(E)$ is identically zero for the Fermi distribution $f(E) = [e^{\frac{E}{T}}+1]^{-1}$ for any T.

It is simple to verify the energy conservation, i.e., that

$$\int_{-\infty}^{\infty} dE\, E I_{\rm ee}(E) = 0. \tag{27}$$

Linearization requires more work, but it is straightforward algebra, which we do not show here. The end result is of the form

$$\delta I_{\rm ee}(E) = \int dE\, M^{\rm ee}_{E\tilde{E}} \varphi_{\tilde{E}} \tag{28}$$

with manifestly real-symmetric integration kernel $M^{\rm ee}_{E\tilde{E}}$.

III. FULL KINETIC EQUATION

As we discuss in more detail in Sec. III below, the electron-phonon kinetic equation,

$$(1-\Sigma')\dot{f} + f'\dot{\Sigma} = I_{\rm ep}, \tag{29}$$

is derived (as usual for the kinetic framework) under the assumption that the electron distribution function $f(E,t)$ varies in time sufficiently slowly.

On the other hand, we saw that as we approach the instability from the right and for $\lambda > \lambda_c$ some of the generalized eigenvalues γ diverge (Fig. 2 in the main text). The corresponding eigenmodes change in time very fast, and the gradient expansion is not valid for them. However, this does not affect the existence of the instability. First, in a stable system all fast modes quickly decay and its long-time dynamics is still governed by Eq. (29). If the exact dynamics is stable, we expect Eq. (29) to be stable too. Otherwise, the fast modes decay until the dynamics is described by Eq. (29) and then grow until Eq. (29) is no longer valid. Thus, the system oscillates perpetually instead of relaxing to the thermal equilibrium. Second, we see from the analysis of the kinetic equation in the strong coupling regime [see, for example, Eq. (8) in the main text] that if the initial deviation from the equilibrium is very smooth in energy (varies little with E), its initial unstable dynamics is correspondingly very slow and is therefore accurately described by Eq. (29).

To simulate the full kinetic equation (29), we use the same discrete energy grid as in Sec. II. This converts Eq. (29) into a differential algebraic equation (DAE) of the form

$$\mathbb{G}\left(\dot{\boldsymbol{f}}, \boldsymbol{f}\right) = 0, \tag{30}$$

where $\boldsymbol{f}$ is an L-dimensional vector $\{f(\epsilon,t), f(2\epsilon,t), \ldots, f(L\epsilon,t)\}$ and $\dot{\boldsymbol{f}}$ denotes the time derivative of $\boldsymbol{f}$. To obtain the above equation, we used the particle-hole symmetry and the following boundary condition:

$$f(0,t) = \frac{1}{2}, \qquad f(j\epsilon,t) = 0, \quad \text{if } j > L. \tag{31}$$

Instead of rewriting the DAE (30) as an ordinary differential equation, we directly solved Eq. (30) using the package `Sundials.jl`. This wrapper package in turn imports solvers from the `SUNDIALS` integrator package [34, 35] that can be implemented using the `Julia` programming language. These solvers are particularly suitable for the kind of nonlinear and stiff differential equation that we have in (30).

We integrate Eq. (30) with the boundary condition (31) and the initial condition

$$\boldsymbol{f}(t=0) = \{f_0(\epsilon, T_{\rm in}), f_0(2\epsilon, T_{\rm in}), \ldots, f_0(L\epsilon, T_{\rm in})\}, \tag{32}$$

where f_0 is the equilibrium Fermi distribution with a temperature $T_{\rm in}$ slightly higher than the phonon temperature T_0, using the `SUNDIALS` DAE solver `IDA` [36]. In this algorithm, the time derivatives at the $n^{\rm th}$ time step t_n are written using the backward differentiation formula of order q as

$$\dot{\boldsymbol{f}}(t_n) = \frac{1}{h_n}\sum_{i=0}^{q} \alpha_{n,i} \boldsymbol{f}(t_{n-i}), \tag{33}$$

where $h_n = t_n - t_{n-1}$, q ranges from 1 to 5, and the coefficients $\alpha_{n,i}$ are uniquely determined by the order q. Applying the above formula to Eq. (30), we reduce the original DAE problem to the problem of solving a nonlinear algebraic system by Newton's method at each time step. Given the initial condition $\boldsymbol{f}(t_0)$, one has to use $q=1$ to obtain $\boldsymbol{f}(t_1)$. Then the step size h_n and the order q are selected after a local error test [36]. For instance, it is possible to use $q=2$ to calculate $\boldsymbol{f}(t_2)$.

As has been mentioned in the main text, see Fig. 1, one ends up having rapidly oscillating solutions – especially close to the

zeros of $Z_0^{-1}(E)$ – when $\lambda > \lambda_c$. This is also seen when one numerically simulates the simplified kinetic equation [Eq. (8) of the main text] in the strong coupling limit. As a result, after a few time steps, the `IDA` integrator fails the local error test too many times [36, 37]. This makes either $q > q_{\max}$ or $h_n < h_{\min}$. At this point, `IDA` stops and returns a give-up message. If $\lambda < \lambda_c$, the simulation of Eq. (29) runs until the provided end-times and obtains

$$\boldsymbol{f}(t = t_{\text{end}}) = \{f_0(\epsilon, T_0), f_0(2\epsilon, T_0), \ldots, f_0(L\epsilon, T_0)\}. \tag{34}$$

IV. KINETIC EQUATION: SHORT REVIEW

The electron-phonon kinetic equation (29) employed in this work forms the backbone of the theory of nonequilibrium phenomena in metals, playing a role analogous to that of Maxwell's equations in electromagnetism. In its modern formulation, it is derived from the Dyson equation in the Keldysh formalism [33, 38] under two principal assumptions: (a) the ions are much slower than the electrons, i.e., the maximum phonon frequency $\Omega \ll E_F$, and (b) the electron distribution function $f(E, t)$ varies sufficiently slowly in time. These conditions justify a gradient expansion and the use of Migdal–Eliashberg theory, even for strong renormalized electron-phonon coupling $\lambda \gtrsim 1$, as long as $\Omega/E_F \ll 1$ [11, 39, 40].

The first step is a gradient expansion of the Dyson equation in the Wigner representation with respect to relative frequency and momentum. Assuming the so-called parameter of the kinetic equation, $\tau_f E_\Sigma \gg 1$, where τ_f and E_Σ are the characteristic time and energy scales over which f and the self-energy Σ vary, it is justified to retain only the leading term — the Poisson bracket

$$\{f, \Sigma\} = f'\dot{\Sigma} - \Sigma'\dot{f}, \tag{35}$$

on the left-hand side of the kinetic equation [40].

Next, one integrates over the single-particle energy $\xi_{\boldsymbol{p}}$. In the limit $\Omega/E_F \to 0$, the self-energy Σ becomes momentum-independent, and the electron-phonon interaction scatters electrons from one point on the Fermi surface to another. Then, the summation over the phonon momentum $\boldsymbol{q}$ in the electron-phonon collision integral reduces to

$$\sum_{\boldsymbol{q}} \frac{g_{\boldsymbol{q}}^2}{2\omega_{\boldsymbol{q}}} \delta(\omega - \omega_{\boldsymbol{q}}) \int \frac{d\Omega'}{4\pi} \delta(\boldsymbol{k}_F - \boldsymbol{k}'_F - \boldsymbol{q}) \equiv \alpha^2 F(\omega), \tag{36}$$

where $g_{\boldsymbol{q}}$ is the electron-phonon matrix element and $\omega_{\boldsymbol{q}}$ is the phonon frequency [21–23, 42]. The left-hand side defines the Eliashberg spectral function $\alpha^2 F(\omega)$.

The kinetic equation then takes the form

$$(1 - \Sigma')\dot{f} + f'\dot{\Sigma} + \boldsymbol{v}_F \cdot \nabla f = I_{\text{ep}}, \tag{37}$$

where I_{ep} is the electron-phonon collision integral:

$$I_{\text{ep}} = 2\pi \int_0^\infty d\omega\, \alpha^2 F(\omega) \left[N(\omega)(f_+ + f_- - 2f) - f(f_+ - f_-) + f_+ - f\right], \tag{38}$$

with $f_\pm = f(E \pm \omega)$ and $N(\omega)$ the phonon distribution function. Note that the dimensionful electron-phonon coupling $g_{\boldsymbol{q}}$ is averaged over the Fermi surface in $\alpha^2 F(\omega)$; thus, its detailed momentum dependence does not affect the dynamics of the electron distribution to leading order in Ω/E_F [33, 38].

This kinetic equation has been derived within the conserving approximation framework [33, 40], and ensures energy and particle number conservation when Σ is determined self-consistently. In equilibrium, the Fermi–Dirac distribution $f_0(E, T_0)$ is a stationary solution, and the quasiparticle weight $Z_0^{-1}(E) = 1 - \Sigma'[f_0]$ emerges naturally from the formalism.

It is important to emphasize that our kinetic approach bypasses the issue of phonon renormalization within electron-phonon models (see the introductory part of the main text). The kinetic equation treats the physical phonon spectrum $\omega_{\boldsymbol{q}}$ and the dimensionful electron-phonon coupling $g_{\boldsymbol{q}}$ as inputs. The goal of our work is to establish a stability constraint on these quantities, irrespective of how they are obtained — whether from experiment, ab initio calculations, or self-consistently from an electron-phonon Hamiltonian, as in Prange and Kadanoff (1964) [11].

On the timescale relevant to the instability, the phonon subsystem remains close to equilibrium (see below), so dynamical phonon feedback is negligible. Accordingly, there is no need for a separate kinetic equation for phonons: the influence of lattice dynamics is already encoded in the renormalized inputs. This standard kinetic treatment is well-suited to our purpose, which is to determine the onset of instability as a function of the physical coupling strength, regardless of how that coupling is determined.

In this work, we consider spatially uniform deviations of the electron distribution function from equilibrium. Then, the spatial gradient term $\boldsymbol{v}_F \cdot \nabla f$ on the left-hand side vanishes, and the distribution evolves according to Eq. (29).

Recall that in our proof that $C_{\text{el}} < 0$ is a sufficient condition for instability, we assumed the initial electron distribution was the (spatially uniform) thermal distribution at temperature T_{in} slightly above the lattice temperature T_0. In linear stability analysis, the specific initial condition is irrelevant: the system is unstable as long as there exists a single unstable normal mode, and stable otherwise.

Even though the initial dynamics of the instability are spatially uniform (as in, e.g., the superconducting instability, which is also translationally invariant), spatial structure can emerge at later times due to coupling between degrees of freedom at different length scales, a common feature in nonlinear media.

In charge density wave systems, for example, a Fermi-surface instability leads to a periodic modulation of both the electronic charge and the lattice distortion [41]. In high-pressure hydrides, such as H_3S, LaH_{10}, and YH_9, strong electron-phonon coupling can induce dynamical instabilities in high-symmetry phases that resolve into distorted or modulated structures [43–50]. Similarly, post-quench dynamics in superconductors can exhibit the spontaneous formation of spatial inhomogeneities due to parametric excitation of pairing modes and the onset of Cooper pair turbulence [51–55]. These effects are often understood as secondary instabilities

or modulational instabilities, and are sometimes described by wave turbulence phenomenology [56].

The investigation of such late-time spatial structure lies beyond the scope of this work. Our goal here is to demonstrate the existence of the instability itself. Since its onset is spatially uniform, it is sufficient for our purposes to analyze the dynamics in the homogeneous setting. The nonlinear spatial evolution following the instability is an interesting direction for future research.

Finally, we comment on the widely used equilibrium phonon approximation, which we have also adopted in this work. This approximation is well justified by the separation of energy and time scales between the electron and phonon subsystems [31, 33, 57–59]. At relevant temperatures, the phonon specific heat exceeds the electronic specific heat by a large factor, $C_{\rm ph}/|C_{\rm el}| \sim E_F/\Omega$, which typically ranges from 10^2 to 10^4 in metals. As a result, the lattice can absorb energy from electrons with minimal change in its distribution and effectively serves as a thermal reservoir. In addition, the phonon-electron collision integral — responsible for driving phonons out of equilibrium — is smaller than the electron-phonon one by a factor of $T/E_F \sim \Omega/E_F$ [31], making the dynamics of phonon distribution much slower. Consequently, it remains near the initial equilibrium on the timescale relevant to the instability.

Effects that fall outside the equilibrium phonon approximation, such as phonon drag (which is parametrically small in metals [60]) or phonon bottlenecks in polar semiconductors [61], are irrelevant in our context. Moreover, although the phonon distribution may evolve at later times — for instance, through heating or structural transitions in hydrides — such processes occur only after the instability has already developed. Since our goal is to establish the existence of the instability and analyze its early-time dynamics, the equilibrium phonon approximation remains fully adequate for our purposes.

V. BENCHMARKING THE KINETIC EQUATION

Because our main results are based on the electron-phonon kinetic equation (29) it is important to put our study into the context of other applications of this equation. In particular, we must demonstrate that the kinetic equation accurately captures phenomena where the quasiparticle weight $Z^{-1} = 1 - \Sigma'$ plays a central role, as it does in our instability analysis. To this end, we review the derivation of the kinetic equation (29) and key benchmark cases where it has been successfully tested against experiment and alternative theoretical approaches.

Applications of the kinetic equation where the quasiparticle weight Z^{-1} plays a central role are numerous and span a wide range of materials, including normal metals, semiconductors, and superconductors. Both the structure of the kinetic equation and the critical role of the quasiparticle weight have been extensively validated through comparisons with experimental data and alternative theoretical approaches. Below, we highlight several representative examples where these validations are particularly direct and relevant to the present work.

One of the earliest explicit uses of the kinetic equation was by Prange and Kadanoff in 1964 in their study of normal metals [11]. Using this equation, they demonstrated that steady-state transport coefficients (such as electrical and thermal conductivities and spin diffusion) are unaffected by electron-phonon many-body corrections to leading order. This explained why conventional Boltzmann theory—which neglects the energy-time Poisson bracket, $\{f, \Sigma\} = f'\dot{\Sigma} - \Sigma' \dot{f}$—successfully accounted for experimental transport measurements, thereby validating its consistency with many-body theory. This provides an early and important confirmation that the kinetic equation correctly incorporates key many-body effects, including the quasiparticle weight.

In the same work, Prange and Kadanoff also derived the expression for the electronic specific heat, which matches experimental results within a few percent accuracy [62–65]. Notably, this expression directly follows from the left-hand side of the kinetic equation, and the quasiparticle weight, together with the $\Sigma' \dot{f}$ term, plays an essential role. Without these contributions, the specific heat would simply correspond to that of free electrons, inconsistent with experimental observations. Thus, the kinetic equation captures the essential renormalization effects responsible for the accurate description of thermodynamic properties.

Another benchmark is the high-field Nernst-Ettingshausen effect, which relates the current density to the vector product of the temperature gradient and the magnetic field. The kinetic equation (with a minor modification to include magnetic field terms) predicts the enhancement of the Nernst-Ettingshausen coefficient by a factor of $Z^{-1} = 1 - \Sigma'$, in good agreement with thermopower measurements.

A third important example is the derivation by Allen [58] of the hot-electron relaxation rate in metals from the kinetic equation, explicitly retaining the quasiparticle renormalization via the electron-phonon coupling constant $\lambda = -\Sigma'|_{E=0}$. His prediction that the relaxation time is proportional to $\lambda\langle\omega^2\rangle$, where $\langle\omega^2\rangle$ is the average squared phonon frequency, was subsequently confirmed by ultrafast pump-probe experiments [66]. These experiments provided a new and accurate method to measure the electron-phonon coupling strength in metals, once again validating the predictive power of the kinetic equation.

Taken together, these examples demonstrate that the kinetic equation reliably captures the key physical phenomena associated with electron-phonon interactions, even when quasiparticle weight renormalization plays a decisive role. Effects originating from the quasiparticle weight, such as those described above and the instability uncovered in our work, are therefore not artifacts of the kinetic theory.

Therefore, the instability we uncover reflects a genuine physical effect, not a shortcoming of the kinetic equation. The logic of our proof is as follows. Assuming the system is a stable metal with a large Fermi energy, the kinetic equation must apply as the appropriate low-energy description. However, it then follows from the kinetic equation that the system becomes unstable once the renormalized electron-phonon coupling exceeds a certain threshold. This establishes that a

metallic state with such a coupling strength cannot be realized physically. The conclusion follows by proof through contradiction.

VI. STRONG COUPLING REGIME

Let us estimate the energy uncertainty ΔE in the strong coupling regime $T \gg \Omega$ for Einstein phonons with frequency Ω. This uncertainty is of the order of the inverse dephasing time τ_ϕ. The electron-phonon collision time in this regime is $\tau \sim (\lambda T)^{-1}$, see, e.g., [22]. The change in electron energy in each collision is very small, of the order of Ω. Modeling the electron energy dynamics as a 1D random walk with a step Ω, we estimate that over the dephasing time the energy changes by

$$\Delta E \sim \Omega \sqrt{\frac{\tau_\phi}{\tau}}. \tag{39}$$

Since, on the other hand, $\Delta E \sim \tau_\phi^{-1}$, equating these two expressions, we obtain

$$\Delta E \sim (g^2 T)^{1/3}. \tag{40}$$

Since the Eliashberg theory is independent of the phonon spectrum in the strong coupling limit, we expect this formula for ΔE to hold for general phonon dispersion, not just Einstein phonons.

The expression for Z_0^{-1} in the strong coupling limit obtains from Eq. (5) of the main text by taking the limit $\omega \to 0$ under the integral. We have

$$\frac{1}{Z_0(E)} = 1 - \frac{g^2}{4\pi^2 T_0^2} \mathrm{Re}\left[\psi^{(2)}\left(\frac{1}{2} + \frac{iE}{2\pi T_0}\right)\right]. \tag{41}$$

Here and in Eq. (40) we restored g for clarity (recall that we are using the energy units where $g = 1$). The length of the interval where $Z_0^{-1} < 0$ is $\delta E = (1.16 - 0.40)g = 0.76g$, which is parametrically larger than the energy uncertainty (40) at temperatures $T \ll g$. Already at $T = T_c = 0.1827g$, we have $\delta E > (g^2 T)^{1/3} = 0.57g$.

[1] R. P. Feynman and F. L. Vernon Jr., The theory of a general quantum system interacting with a linear dissipative system, Ann. Phys. **24**, 118 (1963).

[2] R. P. Feynman, *Statistical Mechanics* (Westview Press, 1998), p. 82.

[3] A. O. Caldeira and A. J. Leggett, Quantum tunnelling in a dissipative system, Ann. Phys. **149**, 374 (1983).

[4] R. Görlich and U. Weiss, Specific heat of the dissipative two-state system, Phys. Rev. B **38**, 5245 (1988).

[5] G.-L. Ingold, P. Hänggi, and P. Talkner, Specific heat anomalies of open quantum systems, Phys. Rev. E **79**, 061105 (2009).

[6] E. A. Yuzbashyan and B. L. Altshuler, Migdal-Eliashberg theory as a classical spin chain, Phys. Rev. B **106**, 014512 (2022).

[7] E. A. Yuzbashyan and B. L. Altshuler, Breakdown of the Migdal-Eliashberg theory and a theory of lattice-fermionic superfluidity, Phys. Rev. B **106**, 054518 (2022).

[8] E. A. Yuzbashyan, M. K. -H. Kiessling, and B. L. Altshuler, Superconductivity near a quantum critical point in the extreme retardation regime, Phys. Rev. B **106**, 064502 (2022).

[9] S.-S. Zhang, Y-M. Wu, A. Abanov, and A. V. Chubukov, Superconductivity out of a non-Fermi liquid. Free energy analysis, Phys. Rev. B 106, 144513 (2022).

[10] S.-S. Zhang, E. Berg, and A. V. Chubukov, Free energy and specific heat near a quantum critical point of a metal, Phys. Rev. B 107, 144507 (2023).

[11] R. E. Prange and L. P. Kadanoff, Transport Theory for Electron-Phonon Interactions in Metals, Phys. Rev. **134**, A566 (1964).

[12] G. Grimvall, *The Electron-Phonon Interaction in Metals* (North-Holland Pub. Co., 1981) p. 125.

[13] W. Lee and D. Rainer, Comment on Eliashberg's free energy of a strong-coupling metal, Z. Physik B - Condensed Matter **73**, 149 (1988).

[14] H. Kleinert, *Path Integrals in Quantum Mechanics, Statistics, Polymer Physics, and Financial Markets* (World Scientific, Singapore, 2009).

[15] J. W. Negele, H. Orland, *Quantum Many-particle Systems* (Perseus Books, 1998).

[16] A. Atland and B. Simons, Condensed Matter Field Theory (Cambridge University Press, 2nd ed., 2010) p. 168 and footnote 13 on p. 171

[17] S. W. Hawking, Zeta function regularization of path integrals in curved spacetime, Commun. Math. Phys. **55**, 133 (1977).

[18] A. Bytsenko, G. Cognola, E. Elizalde, V. Moretti and S. Zerbini, *Analytic Aspects of Quantum Fields* (World Scientific Publishing, 2003).

[19] Zeta-function method for regularization. Encyclopedia of Mathematics.

[20] P. Coleman, *Introduction to Many-Body Physics* (Cambridge University Press, 2015).

[21] P. B. Allen and R. C. Dynes, Transition temperature of strong-coupled superconductors reanalyzed, Phys. Rev. B **12**, 905 (1975).

[22] P. B. Allen and B. Mitrovic, *Theory of superconducting* T_c, in Solid State Physics, edited by H. Ehrenreich, F. Seitz, and D. Turnbull (Academic, New York, 1982), Vol. 37, p. 1.

[23] J.P. Carbotte, Properties of boson-exchange superconductors, Rev. Mod. Phys. **62**, 1027 (1990).

[24] Zhang *et al.* evaluate the total specific heat $C = C_{\rm el} + C_{\rm ph}$, which they denote $C_{\rm ep}$. However, since the specific heat $C_{\rm ph} = \left(\frac{\Omega}{2T}\right)^2 \sinh^{-2}\left(\frac{\Omega}{2T}\right)$ (per lattice site) of Einstein phonons is readily available [25], $C_{\rm el} = C - C_{\rm ph}$ immediately follows. As discussed below Eq. (1) and in [6, 7, 10, 13], Ω here is the renormalized (rather than bare) phonon frequency.

[25] C. Kittel, Introduction to Solid State Physics (John Wiley & Sons, 8th ed., 2005) p. 117

[26] S.V. Shulga, O.V. Dolgov and I. I. Mazin, Electron-phonon coupling and specific heat in $YBa_2Cu_3O_7$, Physica C **192**, 41 (1992).

[27] Golubov *et al.*, Specific heat of MgB_2 in a one- and a two-band model from first-principles calculations, J. Phys.: Condens. Matter **14**, 1353 (2002).

[28] P. T. Landsberg, *Thermodynamics and Statistical Mechanics*

(Dover Publications, 1990), p. 225.
[29] W. Thirring, Systems with negative specific heat, Z. Phys. **235**, 339 (1970).
[30] D. Lynden-Bell and R. M. Lynden-Bell, On the negative specific heat paradox, Mon. Not. R. Astron. Soc. **181**, 405 (1977).
[31] L. P. Pitaevskii and E. M. Lifshitz, *Physical Kinetics: Volume 10* (Butterworth-Heinemann; 1st edition, 1981).
[32] A. Levchenko and J. Schmalian, Transport properties of strongly coupled electron-phonon liquids, Ann. Phys. **419**, 168218 (2020).
[33] J. Rammer and H. Smith, Quantum field-theoretical methods in transport theory of metals, Rev. Mod. Phys. **58**, 323 (1986).
[34] D. J. Gardner, D. R. Reynolds, C. S. Woodward, and C. J. Balos, Enabling new flexibility in the SUNDIALS suite of nonlinear and differential/algebraic equation solvers, ACM Transactions on Mathematical Software (TOMS) **48**, 1–24 (2022).
[35] A. C. Hindmarsh, P. N. Brown, K. E. Grant, S. L. Lee, R. Serban, D. E. Shumaker, and C. S. Woodward, SUNDIALS: Suite of nonlinear and differential/algebraic equation solvers, ACM Transactions on Mathematical Software (TOMS) **31**, 363–396 (2005).
[36] User Documentation for IDA.
[37] K. E. Brenan, S. L. Campbell, and L. R. Petzold, *Numerical Solution of Initial-Value Problems in Differential-Algebraic Equations*, North-Holland, New York (1989).
[38] L. V. Keldysh, Diagram technique for nonequilibrium processes, Sov. Phys. JETP **20**, 1018 (1965).
[39] A. B. Migdal, Interaction between Electrons and Lattice Vibrations in a Normal Metal, Zh. Eksp. Teor. Fiz. **34**, 1438 (1958) [Sov. Phys.–JETP **7**, 996 (1958)].
[40] G. Baym and L. P. Kadanoff, Conservation laws and correlation functions, Phys. Rev. **124**, 287 (1961).
[41] G. Grüner, The dynamics of charge-density waves, Rev. Mod. Phys. **60**, 1129 (1988).
[42] F. Marsiglio and J.P. Carbotte, *Electron-Phonon Superconductivity*, in K. H. Bennemann and J. B. Ketterson, (eds) Superconductivity. (Springer, Berlin, Heidelberg, 2008).
[43] A. P. Drozdov, M. I. Eremets, I. A. Troyan, V. Ksenofontov and S. I. Shylin, Conventional superconductivity at 203 Kelvin at high pressures in the sulfur hydride system, Nature **525**, 73 (2015).
[44] I. Errea *et al.*, Quantum hydrogen-bond symmetrization in the superconducting hydrogen sulfide system, Nature **532**, 81 (2016).
[45] V. S. Minkov, V. B. Prakapenka, E. Greenberg and M. I. Eremets, A Boosted Critical Temperature of 166 K in Superconducting D_3S Synthesized from Elemental Sulfur and Hydrogen, Angew. Chem., Int. Ed. **59**, 18970 (2020).
[46] W. Chen *et al.*, High-Temperature Superconducting Phases in Cerium Superhydride with a Tc up to 115 K below a Pressure of 1 Megabar, Phys. Rev. Lett. **127**, 117001 (2021).
[47] P. Kong *et al.*, Superconductivity up to 243 K in the yttrium-hydrogen system under high pressure, Nat. Commun. **12**, 5075 (2021).
[48] J. Bi *et al.*, Giant enhancement of superconducting critical temperature in substitutional alloy (La,Ce)H_9, Nat. Commun. 13, 5952, (2022).
[49] W. Chen *et al.*, Enhancement of superconducting critical temperature realized in La-Ce-H system at moderate pressures, Nat. Commun. **14**, 2660 (2023).
[50] D. V. Semenok, B. L. Altshuler, E. A. Yuzbashyan, Fundamental limits on the electron-phonon coupling and superconducting T_c, arXiv:2407.12922 (2024).
[51] M. Dzero, E. A. Yuzbashyan, and B. L. Altshuler, Cooper pair turbulence in atomic Fermi gases, EPL **85**, 20004 (2009).
[52] G.-W. Chern and K. Barros, Nonequilibrium dynamics of superconductivity in the attractive Hubbard model, Phys. Rev. B 99, 035162 (2019).
[53] A. Bulgac, Y.-L. Luo, and K. J. Roche, Real-time dynamics of Cooper pairing in strongly interacting Fermi gases, Phys. Rev. Lett. **124**, 062701 (2020).
[54] L. Yang, Y. Yang, and G.-W. Chern, Pattern formation in charge density wave states after a quantum quench, Phys. Rev. B **109**, 195133 (2024).
[55] B. Fan, Z. Cai, and A. M. Garcia-Garcia, Emergence of spatial patterns and synchronization in superconducting time crystals, Phys. Rev. B **110**, 134307 (2024).
[56] V. E. Zakharov, V. S. L'vov, and G. Falkovich, *Kolmogorov Spectra of Turbulence I: Wave Turbulence*, Springer-Verlag, Berlin (1992).
[57] A. A. Abrikosov, *Fundamentals of the Theory of Metals* (Dover Publications, 1988).
[58] P. B. Allen, Theory of thermal relaxation of electrons in metals, Phys. Rev. Lett. **59**, 1460 (1987).
[59] G. M. Eliashberg, Inelastic electron collisions and nonequilibrium stationary states in superconductors, Zh. Eksp. Teor. Fiz. **61**, 1254 (1971) [Sov. Phys.–JETP **34**, 668 (1972)].
[60] See, e.g., Section 81 in [31].
[61] Y. Zou, H. Esmaielpour, D. Suchet et al., The role of nonequilibrium LO phonons, Pauli exclusion, and intervalley pathways on the relaxation of hot carriers in InGaAs/InGaAsP multi-quantum-wells, Sci Rep **13**, 5601 (2023).
[62] F. Marsiglio and J.P. Carbotte, *Electron-Phonon Superconductivity*, in K. H. Bennemann and J. B. Ketterson, (eds) Superconductivity. (Springer, Berlin, Heidelberg, 2008).
[63] J. P. Carbotte, Properties of boson-exchange superconductors, Rev. Mod. Phys. **62**, 1027 (1990).
[64] A. Subedi, L. Ortenzi, and L. Boeri, Electron-phonon superconductivity in APt_3P (A = Sr, Ca, La) compounds: From weak to strong coupling, Phys. Rev. B **87**, 144504 (2013).
[65] A. A. Golubov et al, Specific heat of MgB_2 in a one- and a two-band model from first-principles calculations, J. Phys.: Condens. Matter **14**, 1353 (2002).
[66] S. D. Brorson et al., Femtosecond room-temperature measurement of the electron-phonon coupling constant λ in metallic superconductors," Phys. Rev. Lett. **64**, 2172 (1990).